ATLAS NOTE

ATLAS-CONF-2011-100

October 5, 2011

Measurement of the top-quark pair production cross-section in pp collisions at $\sqrt{s} = 7$ TeV in dilepton final states with ATLAS

The ATLAS Collaboration

Abstract

A measurement of the production cross-section of top-quark pairs ($t\bar{t}$) in proton-proton collisions at a center-of-mass energy of 7 TeV recorded with the ATLAS detector at the Large Hadron Collider is reported. Candidate events are selected in the dilepton topology with large missing transverse energy and at least two jets. Using a data sample corresponding to an integrated luminosity of 0.70 fb^{-1}, a $t\bar{t}$ production cross-section $\sigma_{t\bar{t}} = 177 \pm 6(\text{stat.})^{+17}_{-14}(\text{syst.}) \pm 8(\text{lum.})$ pb is measured for an assumed top-quark mass of $m_t = 172.5$ GeV. A second measurement requiring at least one jet consistent with arising from a b quark yields $\sigma_{t\bar{t}} = 183 \pm 6(\text{stat.})^{+18}_{-14}(\text{syst.})^{+8}_{-7}(\text{lum.})$ pb. These measurements are in good agreement with each other and with Standard Model predictions.

1 Introduction

As the heaviest known elementary particle, the top quark is a particularly interesting probe of the Standard Model (SM).The measurement of the $t\bar{t}$ production cross-section is a sensitive test of perturbative QCD and the SM description of top-quark decay. The production cross-section in proton-proton (pp) collisions at a center-of-mass energy $\sqrt{s} = 7$ TeV is predicted to be 165^{+11}_{-16} pb at approx. NNLO [1, 2], and the top quark is predicted to decay nearly 100% of the time to a W boson and a bottom quark. A measured cross-section that differs significantly from the SM prediction can be a sign of new physics in either the production, or the decay. Furthermore, $t\bar{t}$ production is an important background in many searches for physics beyond the SM, and in searches for SM Higgs boson.

Within the SM, the $t\bar{t}$ event topologies are determined by the decays of the two W bosons. In increasing order of $t\bar{t}$ branching fraction: dilepton final states occur when both W bosons decay to a charged-lepton and a neutrino, 'lepton plus jets' final states when only one W boson decays leptonically, while the other decays to a pair of quarks, and all-hadronic final states when both W bosons decay to pairs of quarks.

Top-quark production in dilepton final states has been studied using proton-antiproton collisions at $\sqrt{s} = 1.96$ TeV [3, 4] and LHC measurements have recently been reported [5, 6]. We present a measurement of the $t\bar{t}$ production cross-section using the dilepton channel, characterized by two opposite-sign leptons, unbalanced transverse momentum indicating the presence of neutrinos from the W-boson decays and two b-quark jets. The measurement is performed with twenty times more data than our previous measurement of $t\bar{t}$ production [7].

The $t\bar{t}$ dilepton final states can be selected with a good signal-to-background ratio using simple kinematic requirements on the final-state objects. With the additional requirement of the presence of a jet consistent with arising from a b quark ('b-tag'), the signal-to-background ratio can be further improved. Cross-section measurements with and without the b-tag requirement are reported here in which the leptons include both reconstructed electrons and muons. Tau leptons are not explicitly reconstructed, but reconstructed electrons or muons can arise from leptonic tau decays and these are included in the signal acceptance.

The expected background contributions from Z/γ^*+jets, single top quarks, WW, WZ, and ZZ events, and events with misidentified leptons are subtracted from the number of candidate events and the cross-section is measured taking into account the $t\bar{t}$ signal acceptance. Background contributions from Z/γ^*+jets and events with misidentified leptons are evaluated directly from the data. All other background contributions are evaluated using Monte Carlo simulations.

2 Detector and data sample

The ATLAS detector [8] at the LHC covers nearly the entire solid angle[1] around the collision point. It consists of an inner tracking detector (ID) comprising a silicon pixel detector, a silicon microstrip detector (SCT), and a transition radiation tracker (TRT). The ID is surrounded by a thin superconducting solenoid providing a 2 T magnetic field, and by liquid-argon electromagnetic sampling calorimeters (LAr) with high-granularity. An iron-scintillator tile calorimeter provides hadronic energy measurements in the central rapidity range ($|\eta| < 1.7$). The end-cap and forward regions are instrumented with LAr calorimetry for both electromagnetic and hadronic energy measurements out to $|\eta| < 4.9$. The calorimeter system is surrounded by a muon spectrometer incorporating three superconducting toroid magnet assemblies.

[1] In the right-handed ATLAS coordinate system, the pseudorapidity η is defined as $\eta = -\ln[\tan(\theta/2)]$, where the polar angle θ is measured with respect to the LHC beamline. The azimuthal angle ϕ is measured with respect to the x-axis, which points towards the centre of the LHC ring. The y-axis points up. Transverse momentum and energy are defined as $p_{\mathrm{T}} = p\sin\theta$ and $E_{\mathrm{T}} = E\sin\theta$, respectively.

A three-level trigger system is used to select events for this analysis. The level-1 trigger is implemented in hardware and uses a subset of the detector information to reduce the rate to a design value of at most 75 kHz. This is followed by two software-based trigger levels, that together reduce the event rate to about 200 Hz.

The analysis uses collision data with a center-of-mass energy of $\sqrt{s} = 7$ TeV recorded in 2011, with an integrated luminosity of 0.70 ± 0.03 fb^{-1} [9].

3 Simulated samples

Monte Carlo (MC) simulation samples are used to calculate the $t\bar{t}$ acceptance and to evaluate the background contributions from single top quarks, WW, WZ, and ZZ events, and $Z/\gamma^* \to \tau\tau$. All MC samples are processed with the GEANT4 [10] simulation of the ATLAS detector [11] and events are passed through the same analysis chain as the data.

The generation of $t\bar{t}$ and single top-quark events uses the MC@NLO generator [12, 13, 14] with the CTEQ6.6 [15] parton distribution function (PDF) set and a top-quark mass of 172.5 GeV. The $t\bar{t}$ cross-section is normalized to the prediction of Hathor[16], which employs an approximate next-to-next-to-leading order (NNLO) pertubative QCD calculation. Single top-quark production with MC@NLO includes the s, t and Wt channels and the diagram-removal scheme [17] is used to reduce overlap with the $t\bar{t}$ final state.

Drell-Yan events (Z/γ^*+jets) are modeled with the Alpgen generator, using the MLM matching scheme [18] and the CTEQ6L1 [19] PDF set. The Z/γ^*+jets samples, including both light and heavy flavor jets, are normalized to NNLO with a K-factor of 1.25 [20]. In the $Z/\gamma^* \to ee$ and $\mu\mu$ decay channels, the background from Z/γ^*+jets is evaluated using a data-driven technique that normalizes the MC expectation to the data observation near the Z pole. The background from Z/γ^*+jets is normalized to the data observation near the Z pole. Background contributions from the W+jets final states come primarily from events where the W boson decays leptonically and the second lepton candidate is a misidentified jet or a heavy-flavor decay. Backgrounds from W+jets events are evaluated directly from the data.

All MC simulated events are hadronized using the Herwig shower model [21, 22] supplemented by the Jimmy underlying event model [23]. Both hadronization programs are tuned to ATLAS data using the ATLAS MC10 tune [24]. Diboson events are modeled using the Alpgen generator normalized with K-factors of 1.26 (WW), 1.28 (WZ) and 1.30 (ZZ) to match the total cross-section from NLO QCD predictions using calculations with the MCFM program [25].

All Monte Carlo samples are generated with both in-time and out-of-time pile-up (multiple pp interactions). The MC events are re-weighted so that the distribution of interactions per crossing in the MC matches that observed in the data.

4 Object selection

Leptons are required to be isolated and have high transverse momentum, p_{T}, consistent with their originating from W-boson decay, with p_{T} thresholds chosen to ensure events are triggered with high efficiency.

Electron candidates are reconstructed from energy deposits (clusters) in the EM calorimeter, which are then associated to reconstructed tracks of charged particles in the inner detector. Stringent quality requirements on the conditions of the EM calorimeter are applied to ensure a well measured reconstructed energy. A cut-based selection [26], using calorimeter, tracking and combined variables, is employed to provide good separation between the signal electrons and background. Electron candidates are additionally required to have $p_{\mathrm{T}} > 25$ GeV and $|\eta_{cl}| < 2.47$, excluding electrons from the transition region between the barrel and endcap calorimeters defined by $1.37 < |\eta_{cl}| < 1.52$. The variable η_{cl} is the pseudorapidity of the calorimeter energy cluster associated with the candidate.

Muon candidates are reconstructed by searching for track segments in layers of the muon chambers. These segments are combined starting from the outermost layer, fitted to account for material effects, and matched with tracks found in the inner detector. The candidates are refitted using the complete track information from both detector systems [20], and required to satisfy $p_{\mathrm{T}} > 20$ GeV and $|\eta| < 2.5$.

Both electrons and muons are required to be isolated to reduce background from misidentified jets and to suppress the selection of leptons from heavy-flavor decays. For electron candidates, the transverse energy (E_{T}) deposited in the calorimeter not associated to the electron is summed in a cone in $\eta - \phi$ space of radius $\Delta R = 0.2$ around the electron and required to be less than 3.5 GeV. For muon candidates, both the corresponding calorimeter isolation energy and the analogous track isolation, the sum of the track transverse momenta for tracks with $p_{\mathrm{T}} > 1$ GeV and in a cone $\Delta R = 0.3$ centered on the lepton candidate, must be less than 4 GeV. Additionally, muon candidates must have a distance $\Delta R > 0.4$ from any jet with $p_{\mathrm{T}} > 20$ GeV, further suppressing muon candidates from heavy flavor decays. Muon candidates arising from cosmic rays are rejected by removing candidate pairs that are back-to-back in the $r - \phi$ plane and with transverse impact parameters relative to the beam axis $d_0 > 0.5$ mm.

Jets are reconstructed with the *anti-k_t* algorithm [27] with distance parameter $R = 0.4$ starting from energy clusters of adjacent calorimeter cells. These jets are calibrated by first correcting the jet energy using the scale established for electromagnetic objects and then performing a further correction to the hadronic energy scale using p_{T} and η dependent correction factors obtained from simulation [28]. Jets are removed if they are within $\Delta R = 0.4$ of a well-identified electron candidate. The jets used in the analysis are required to have $p_{\mathrm{T}} > 25$ GeV and $|\eta| < 2.5$.

Jets are identified as b-quark candidates ('b-tagged') by an algorithm that forms a likelihood ratio of b- and light-jet hypothesis using the following discriminating variables: the signed impact parameter significance of well-measured tracks associated with a given jet, the decay length significance measured by reconstructing a secondary vertex, the invariant mass of all tracks associated to the secondary vertex, the ratio of sum of the energies of the tracks associated with the secondary vertex to the sum of the energies of all tracks in the jet, and the number of two-track vertices that can be formed at the secondary vertex. The cut on the combined likelihood ratio has been chosen such that a b-tagging efficiency of $\approx 80\%$ per b-jet in $t\bar{t}$ candidate events is achieved.

The missing transverse energy ($E_{\mathrm{T}}^{\mathrm{miss}}$) is formed from the vector sum of transverse momenta of all jets with $p_{\mathrm{T}} > 20$ GeV and $|\eta| < 4.5$. The contribution from cells associated with electron candidates is replaced by the candidate's calibrated transverse energy. The contribution from all muon candidates and calorimeter clusters not belonging to a reconstructed object is also included.

5 Event selection

The analysis requires collision data selected by an inclusive single lepton trigger (e or μ) that is fully efficient for lepton candidates satisfying $p_{\mathrm{T}} > 25$ GeV. To ensure that the event was triggered by the lepton candidates used in the analysis, one of the leptons and the trigger object are required to match within $\Delta R < 0.15$.

Events are required to have a primary interaction vertex with at least five tracks. The event is discarded if any jet with $p_{\mathrm{T}} > 20$ GeV fails quality cuts designed to reject jets arising from out-of-time activity or calorimeter noise [29]. If an electron candidate and a muon candidate share a track, the event is also discarded.

The selection of events in the signal region consists of a series of kinematic requirements on the reconstructed objects. The requirements on $E_{\mathrm{T}}^{\mathrm{miss}}$, the lepton-lepton invariant mass ($m_{\ell\ell}$), and the scalar p_{T} sum of all selected jets and leptons (H_{T}) are optimized to minimize the expected total uncertainty in the cross-section measurement. The resulting event selection, referred to as the 'non-b-tag' selection, is:

- Events must have exactly two oppositely-charged lepton candidates (ee, $\mu\mu$, $e\mu$).
- Events must have at least two jets with $p_{\mathrm{T}} > 25$ GeV and $|\eta| < 2.5$
- Events are required to have $m_{\ell\ell} > 15$ GeV in order to reject backgrounds from bottom-quark production and vector-meson decays.
- Events in the ee and $\mu\mu$ channels must satisfy $E_{\mathrm{T}}^{\mathrm{miss}} > 60$ GeV, to suppress multijet background, and $m_{\ell\ell}$ must differ by at least 10 GeV from the Z-boson mass, m_Z, to suppress background from Z+jets.
- For the $e\mu$ channel, no $E_{\mathrm{T}}^{\mathrm{miss}}$ or $m_{\ell\ell}$ cuts are applied. In this case, remaining background from Z/γ^*+jets production is suppressed by requiring $H_{\mathrm{T}} > 130$ GeV.

In addition to the non-b-tag selection, a parallel selection with the additional requirement of at least one b-tagged jet is made. This allows for an event selection that can be further optimized for background rejection. Because of the enhanced background rejection, the $E_{\mathrm{T}}^{\mathrm{miss}}$ requirement for ee and $\mu\mu$ events is relaxed to $E_{\mathrm{T}}^{\mathrm{miss}} > 40$ GeV, while the H_{T} requirement for $e\mu$ events is set at $H_{\mathrm{T}} > 140$ GeV, when also requiring at least one b-tagged jet in the event.

6 Backgrounds

The $t\bar{t}$ event selection is designed to reject Z/γ^*+jets events near the dilepton resonances. However, Z/γ^*+jets events with dilepton invariant mass away from the resonance masses can enter the signal region when there is large $E_{\mathrm{T}}^{\mathrm{miss}}$, typically from mismeasurement. These events are difficult to properly model in simulations due to large uncertainties on the non-Gaussian tails of the $E_{\mathrm{T}}^{\mathrm{miss}}$ distribution, on the Z boson cross-section for higher jet multiplicities, and on the lepton energy resolution.

To evaluate the Z/γ^*+jets background in dielectron and dimuon events ($Z \to \tau\tau$ is considered elsewhere), the MC prediction for the number of events in the signal region is normalized to the data using the number of Z/γ^*+jets events measured in a control region [7]. The control region is formed by events with the same jet requirements as the signal region, but with $m_{\ell\ell}$ within 10 GeV of the Z-boson mass, and a $E_{\mathrm{T}}^{\mathrm{miss}}$ cut of $E_{\mathrm{T}}^{\mathrm{miss}} > 30$ GeV. Contamination in the control region from other physics processes (signal and other background processes considered for the analysis) is subtracted according to MC predictions. The ratio of data events to MC expectation in the control region provides a scale factor that is used to correct the MC prediction for Z/γ^*+jets events in the signal region.

Other backgrounds mainly come from W+jets, $t\bar{t}$ single lepton+jets, and single top-quark production with non-prompt leptons. The term 'fake lepton' is used to refer to both misidentified and non-prompt lepton candidates.

The yield of events with fake leptons is evaluated from the data using a matrix method [6]. Categories of events with a combination of two leptons, which either pass lepton identification cuts with looser isolation criteria or the full cuts, are correlated with their sources via a 4×4 matrix. For each real or fake lepton there is a probability to pass not only the loose, but also the full cuts. These probabilities enter the matrix elements such that the number of events with a particular combination of two identified leptons is the sum of the source events multiplied by the probability to form this particular combination.

The probability for real leptons is measured as a function of jet multiplicity using data samples of $Z \to ee$ and $Z \to \mu\mu$ events. The corresponding probability for fake leptons is measured in a data sample dominated by dijet production, with events containing one lepton candidate passing the looser isolation cuts and having low $E_{\mathrm{T}}^{\mathrm{miss}}$. Contributions from real leptons due to W+jets final states are subtracted using simulated events. The matrix is inverted in order to extract the real and fake content of the observed event sample.

The contributions from other electroweak background processes with two real leptons, referred to as 'Other EW', such as single top quarks, $Z \to \tau\tau$, WW, ZZ and WZ production are determined from Monte Carlo simulations. The expected numbers of background events are included in Table 1.

The modeled acceptances, efficiencies and data-driven background evaluation methods are validated by comparing Monte Carlo predictions with data in control regions with kinematics similar to the signal region but dominated by backgrounds. In particular, the $E_{\mathrm{T}}^{\mathrm{miss}}$, $m_{\ell\ell}$ and jet multiplicity distributions in a sample of Z-boson candidates, defined by requiring $|m_{\ell\ell} - m_Z| < 10$ GeV and $E_{\mathrm{T}}^{\mathrm{miss}} < 60$ GeV, are studied. The MC predictions in the control regions are in reasonable agreement with data, although small discrepancies exist in regions that do not affect the $t\bar{t}$ cross-section measurement.

The background contributions for the analysis requiring at least one b-tagged jet are determined using the same techniques described above, with the additional requirement of a b-tagged jet in both signal and control regions.

	ee	$\mu\mu$	$e\mu$	b-tag ee	b-tag $\mu\mu$	b-tag $e\mu$
$Z/\gamma^*(\to ee/\mu\mu)$+jets	$3.8^{+2.5}_{-1.2}$	14.8 ± 4.7	-	$9.3^{+3.7}_{-1.9}$	$19.1^{+2.4}_{-1.6}$	-
$Z/\gamma^*(\to \tau\tau)$+jets	5.2 ± 2.6	11.2 ± 4.8	43 ± 16	$1.6^{+1.1}_{-0.9}$	$7.0^{+2.8}_{-3.2}$	$9.1^{+3.6}_{-3.7}$
Fake leptons	3.1 ± 2.2	$0.3^{+0.6}_{-0.3}$	44 ± 24	4.9 ± 3.1	1.0 ± 0.8	19 ± 12
Single top quarks	6.6 ± 1.2	16.2 ± 2.0	40.9 ± 5.6	$6.8^{+1.3}_{-1.2}$	$15.4^{+2.5}_{-2.4}$	$30.8^{+4.9}_{-4.5}$
Diboson	5.6 ± 1.0	8.2 ± 1.2	30.9 ± 4.6	2.1 ± 0.8	$2.7^{+0.9}_{-0.6}$	$8.7^{+1.5}_{-1.3}$
Total bkg.	$24.3^{+5.4}_{-4.7}$	50.8 ± 8.4	158 ± 34	$24.7^{+5.2}_{-4.0}$	$45.2^{+4.6}_{-4.4}$	68 ± 14
Predicted $t\bar{t}$	130 ± 16	243^{+22}_{-27}	728 ± 59	161 ± 21	304^{+29}_{-37}	644^{+60}_{-74}
Total	154 ± 17	294^{+23}_{-28}	886 ± 68	186 ± 21	349^{+30}_{-37}	712^{+61}_{-75}
Observed	165	287	962	202	349	823

Table 1: Breakdown of the expected $t\bar{t}$ signal and background events in the signal region compared to the observed event yields, for each of the dilepton channels. All systematic uncertainties are included, and correlations between different background sources are taken into account.

7 Systematic uncertainties

Lepton trigger, reconstruction and selection efficiencies are assessed by comparing $Z \to ee$ and $Z \to \mu\mu$ events in the same data sample as used for the $t\bar{t}$ analyses. Scale factors are evaluated by comparing these efficiencies with those determined with simulated Z boson events. The scale factors are applied to MC samples when calculating acceptances to account for any differences between predicted and observed efficiencies. Systematic uncertainties on these scale factors are evaluated by varying the selection of events used in the efficiency measurements and by checking the stability of the measurements over the course of the run.

The modeling of lepton momentum scale and resolution is studied using reconstructed dilepton invariant mass distributions of Z/γ^* candidate events and used to adjust the simulation accordingly. The acceptance uncertainty from the lepton modeling is dominated mostly by the electron selection efficiency uncertainty.

The jet energy scale (JES) and its uncertainty are derived by combining information from test-beam data, LHC collision data and simulation [30]. For jets within the acceptance, the JES uncertainty varies in the range 4–8% as a function of jet p_{T} and η. This uncertainty is somewhat higher than in the previous result [7] because of the additional uncertainty due to multiple pp interactions at high instantaneous

luminosity. The jet energy resolution and jet reconstruction/identification efficiency measured in data and in simulation are in good agreement. The statistical uncertainties on the comparisons, 10% and 1–2% for the energy resolution and the efficiency, respectively, are taken as systematic uncertainties associated with these effects. The effect on the acceptance is dominated by the JES uncertainty.

The systematic uncertainty in the efficiency of the b-tagging algorithm has been estimated to be 6% for b-quark jets, based on b-tagging calibration studies using inclusive lepton and multijet final states. The uncertainties on the tagging efficiencies for light and charm quarks are larger, but are not a large source of uncertainty due to the intrinsically high signal-to-background ratios in the dilepton final states. The acceptance uncertainty due to b-tagging is about 3% for all the three channels.

The uncertainty in the kinematic distributions of the $t\bar{t}$ signal events gives rise to systematic uncertainties in the signal acceptance, with contributions from the choice of generator, the modeling of initial and final state radiation (ISR/FSR) and the PDFs. The generator uncertainty is evaluated by comparing the MC@NLO predictions with those of the POWHEG [31, 32, 33] interfaced to either HERWIG or PYTHIA. The uncertainty due to ISR/FSR is evaluated using the ACERMC generator [34] interfaced to the PYTHIA shower model, and by varying the parameters controlling ISR and FSR in a range consistent with experimental data [20]. Finally, the PDF uncertainty is evaluated using a range of current PDF sets [20]. The dominant uncertainties in this category of systematics are the modeling of ISR/FSR and the generator choice.

The overall normalization uncertainties on the backgrounds from single top-quark and diboson production are taken to be 10%[35, 36] and 5%[37], respectively. The systematic uncertainties from the background evaluations that are taken from the data include the statistical uncertainties in these methods as well as the systematic uncertainties arising from the objects and MC estimates that are used. An uncertainty on the data-driven Z/γ^*+jets evaluation is included in which the $E_{\mathrm{T}}^{\mathrm{miss}}$ cut in the control region is varied by ±5 GeV. The uncertainty on the measured integrated luminosity of the dataset is 3.7%.

Tables 2 and 3 list the contributions to the cross-section measurement of each of the systematic uncertainties considered for the measurements without and with b-tagging, respectively. In the ee channel there are several relatively large uncertainties (jet energy scale, ISR, FSR) that have a contribution from the limited sample size.

8 Cross-section measurement

The expected and measured numbers of events in the signal region, after applying all selection cuts for each of the individual dilepton channels, are shown in Table 1. A total of 1414 candidate events are observed for the analysis without b-tagging, and a total of 1374 candidate events are found for the analysis with b-tagging. There are 1,197 events in common between the two selections.

In Fig. 1 the numbers of selected jets and the expectation for 0.70 fb^{-1} are shown for the non-b-tag analysis, and for the b-tag analysis, with the three channels combined. In the non-b-tag case, all requirements except the jet multiplicity selection are applied, and in the b-tag case all requirements except the b-tag requirement are applied. The distributions of H_{T} are shown in Fig. 2 for the $e\mu$ channel in both b-tagged and non-b-tagged varieties. All requirements except H_{T} are applied. In Figs. 3 and 4 the $E_{\mathrm{T}}^{\mathrm{miss}}$ distribution in ee and $\mu\mu$ events is shown for events passing all signal-region requirements except the $E_{\mathrm{T}}^{\mathrm{miss}}$ selection. The dominant backgrounds are Z/γ^*+jets production and W+jets production with a fake lepton.

The cross-section results are obtained with a likelihood fit in which the number of observed events, N_i^{obs}, in each channel i is modeled as a Poisson distribution, $\mathcal{P}$, of the expected number of signal and background events, $N_{i,\mathrm{tot}}^{\mathrm{exp}}$. The integrated luminosity, L, is modeled with a Gaussian distribution, $\mathcal{G}$, about its central value, L_0. The systematic variation in $N_{i,\mathrm{tot}}^{\mathrm{exp}}$ due to each systematic source j is modeled with a nuisance parameter α_j, where $\alpha_j = \pm 1$ represent the ± one standard deviation variation of the systematic

	ee	$\mu\mu$	$e\mu$	Combined
Uncertainty Source	$\Delta\sigma/\sigma$[%]	$\Delta\sigma/\sigma$[%]	$\Delta\sigma/\sigma$[%]	$\Delta\sigma/\sigma$[%]
Data statistics	-9.3 / 9.8	-6.6 / 6.8	-4.1 / 4.2	-3.3 / 3.3
Luminosity	-4.0 / 4.7	-3.7 / 4.3	-4.3 / 4.7	-4.2 / 4.6
MC statistics	-4.2 / 4.9	-2.8 / 3.2	-1.9 / 2.1	-1.5 / 1.6
Lepton energy scale	0.0 / 0.9	0.0 / 0.5	-0.3 / 0.3	-0.4 / 0.0
Lepton energy resolution	0.0 / 0.6	-0.5 / 0.8	0.0 / 0.5	-0.4 / 0.3
Lepton indent. scale factor	-5.5 / 6.6	-1.2 / 2.7	-3.1 / 3.4	-2.6 / 2.7
Jet energy scale	-10.0 / 10.6	-3.8 / 7.6	-3.7 / 4.5	-5.9 / 5.3
Jet energy resolution	-0.6 / 0.8	-3.1 / 3.6	-0.6 / 0.7	-0.4 / 0.3
Jet reconstr. efficiency	0.0 / 0.0	0.0 / 0.0	0.0 / 0.0	0.0 / 0.0
Drell-Yan prediction	0.0 / 0.0	-0.4 / 0.4	0.0 / 0.0	0.0 / 0.0
Fake leptons	-1.6 / 1.6	-0.4 / 0.4	-3.2 / 3.2	-2.0 / 1.9
MC generator	-4.3 / 5.3	0.0 / 0.0	-2.9 / 3.2	-2.1 / 2.3
Parton shower	-4.7 / 5.8	-0.4 / 0.5	-2.9 / 3.2	-2.3 / 2.4
ISR	-7.1 / 0.6	-0.8 / 3.6	-0.5 / 2.4	-2.4 / 2.5
FSR	-13.6 / 0.6	-0.7 / 4.3	-2.4 / 0.5	-1.3 / 1.4
PDF	-2.4 / 2.8	-1.7 / 2.2	-2.4 / 2.7	-2.3 / 2.5
$E_{\mathrm{T}}^{\mathrm{miss}}$ reconstruction	-1.0 / 1.1	-0.8 / 1.7	0.0 / 0.0	-0.5 / 0.6
Pile-up	-0.6 / 1.3	-0.5 / 1.5	0.0 / 0.0	-0.5 / 0.5
Detector modeling	-0.6 / 1.1	-0.7 / 1.5	-0.7 / 1.2	-1.0 / 1.3
Theoretical cross-sections	-1.4 / 1.3	-1.7 / 1.8	-2.1 / 2.1	-1.9 / 1.9
All systematics	-20 /18	-7.3 /13	-9.2 /11	-9.3 / 10
Stat + Syst	-22 / 20	-9.9 / 15	-10 / 12	-9.8 / 11

Table 2: Overview of the $t\bar{t}$ cross-section uncertainties for each channel, and for the combination, obtained from the likelihood minimization in the non-b-tag analysis.

	ee	$\mu\mu$	$e\mu$	Combined
Uncertainty Source	$\Delta\sigma/\sigma$[%]	$\Delta\sigma/\sigma$[%]	$\Delta\sigma/\sigma$[%]	$\Delta\sigma/\sigma$[%]
Data statistics	-8.3 / 8.7	-5.8 / 6.1	-4.2 / 4.4	-3.2 / 3.3
Luminosity	-3.8 / 4.5	-3.7 / 4.1	-4.3 / 4.7	-4.1 / 4.5
MC statistics	-3.8 / 4.5	-2.6 / 2.9	-2.1 / 2.2	-1.5 / 1.6
Lepton energy scale	-0.7 / 0.0	-0.5 / 0.0	-0.3 / 0.3	-0.3 / 0.3
Lepton energy resolution	0.0 / 0.4	-0.6 / 0.0	0.0 / 0.0	0.0 / 0.3
Lepton ident. scale factor	-5.5 / 6.3	-2.3 / 2.4	-3.1 / 3.4	-2.4 / 2.6
Jet energy scale	-9.7 / 4.8	-4.9 / 5.5	-4.9 / 5.1	-4.7 / 5.3
Jet energy resolution	-1.9 / 2.0	-1.4 / 1.3	-1.4 / 1.4	-1.4 / 1.5
Jet reconstr. efficiency	0.0 / 0.0	-0.6 / 0.0	-0.3 / 0.3	-0.3 / 0.3
Drell-Yan prediction	-0.6 / 0.6	-0.6 / 0.0	0.0 / 0.0	0.0 / 0.0
Fake leptons	-1.9 / 1.8	-0.6 / 0.0	-1.9 / 1.8	-1.1 / 1.2
MC generator	-5.7 / 7.0	-1.3 / 1.3	-2.7 / 2.9	-0.7 / 0.7
Parton shower	-0.6 / 0.0	0.0 / 0.0	0.0 / 4.0	0.0 / 0.3
b-tag efficiency	-3.2 / 4.5	-3.0 / 4.1	-3.5 / 4.7	-3.4 / 4.5
Light quark tag eff.	0.0 / 0.0	-0.6 / 0.0	-0.5 / 0.0	-0.3 / 0.3
ISR	-4.8 / 5.8	-1.5 / 1.5	-0.3 / 0.4	-0.4 / 0.4
FSR	-8.7 / 11.2	-2.8 / 3.1	-0.9 / 0.8	-2.0 / 2.1
PDF	-2.7 / 3.2	-2.3 / 2.5	-2.4 / 2.6	-2.5 / 2.7
$E_{\mathrm{T}}^{\mathrm{miss}}$ reconstruction	-0.9 / 0.0	-1.0 / 0.0	0.0 / 0.0	-0.0 / 0.0
Pile-up	-0.8 / 0.0	-0.3 / 0.0	0.0 / 0.0	-0.0 / 0.0
Detector modeling	-0.7 / 1.4	-0.8 / 2.2	-1.1 / 1.6	-1.9 / 1.8
Theoretical cross-sections	-0.4 / 0.4	-1.1 / 0.6	-0.7 / 0.7	-0.7 / 0.7
All systematics	-16 / 20	-7.9 / 9.9	-8.2 / 11	-8.1 / 9.7
Stat. + Syst.	-19/ 22	-10 / 12	-10 / 13	-9.0 / 11

Table 3: Overview of the $t\bar{t}$ cross-section uncertainties for each channel, and for the combination, obtained from the likelihood minimization in the b-tag analysis.

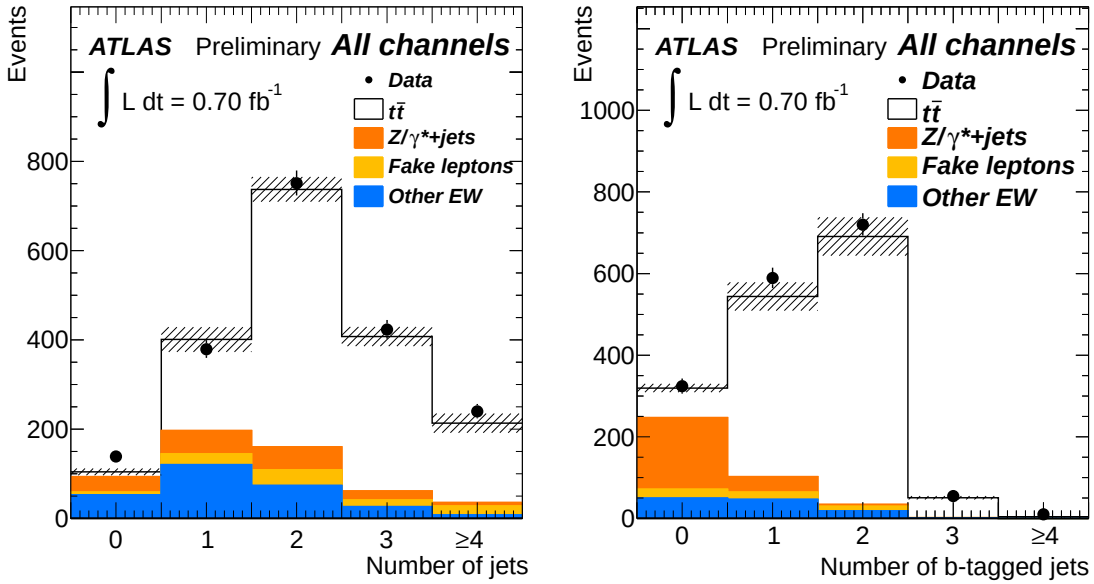

(a) (b)

Figure 1: (a) Jet multiplicity distribution for ee+$\mu\mu$+$e\mu$ events without b-tag. (b) Multiplicity distribution of b-tagged jets in ee+$\mu\mu$+$e\mu$ events. Contributions from diboson and single top-quark events are summarized as 'Other EW'. Note that the events in (b) are not a simple subset of those in (a) because the event selections for the b-tag and non-b-tag analyses differ.

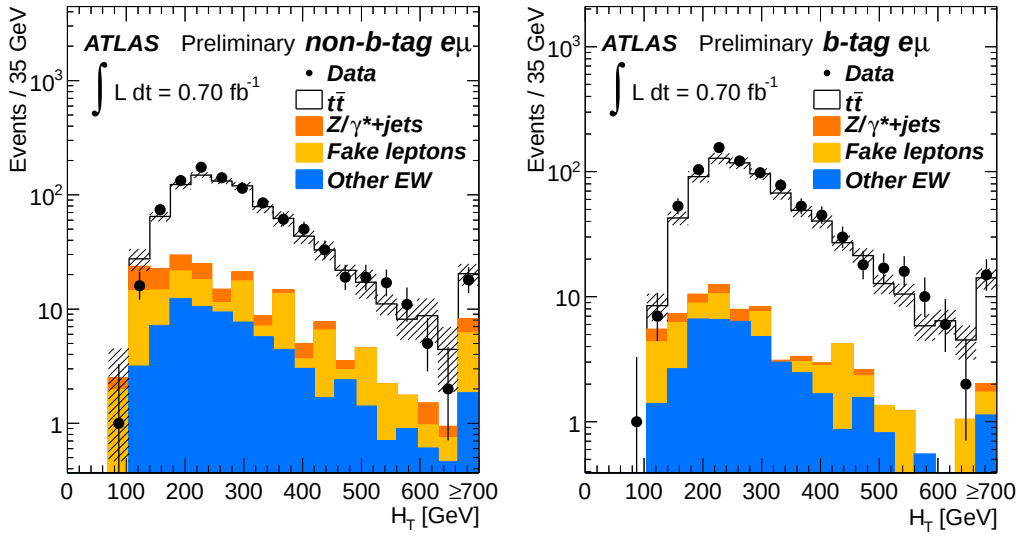

(a) (b)

Figure 2: The H_{T} distribution in the signal region for (a) the non-b-tag $e\mu$ channel, (b) the b-tagged $e\mu$ channel. Contributions from diboson and single top-quark events are summarized as 'Other EW'.

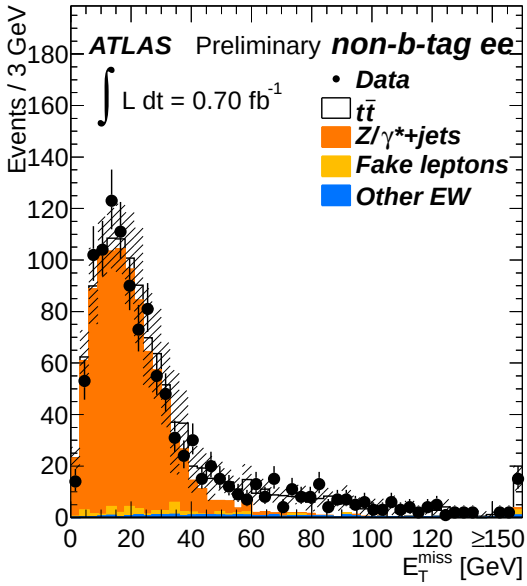

(a)

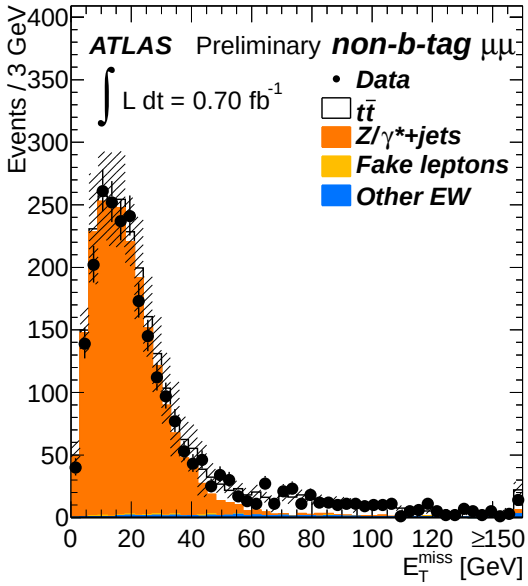

(b)

Figure 3: $E_{\mathrm{T}}^{\mathrm{miss}}$ distribution in ee and $\mu\mu$ events for the non-b-tag signal region, omitting the $E_{\mathrm{T}}^{\mathrm{miss}}$ >60 GeV requirement.

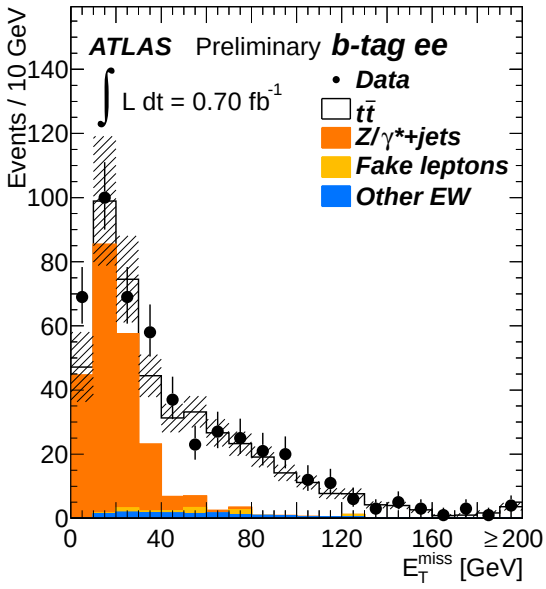

(a)

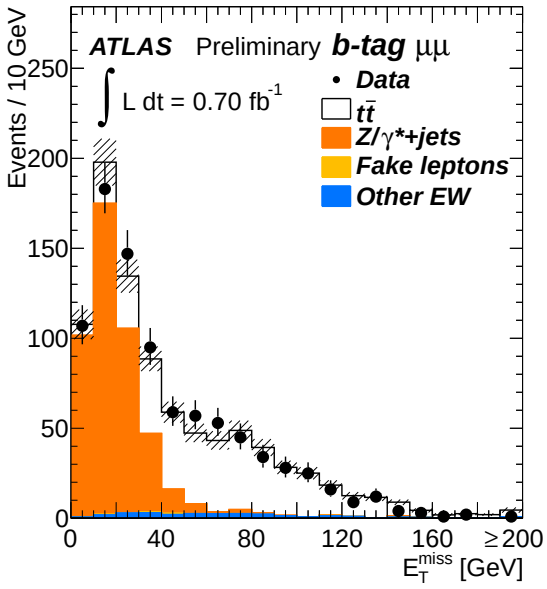

(b)

Figure 4: $E_{\mathrm{T}}^{\mathrm{miss}}$ distribution in ee and $\mu\mu$ events for the b-tag signal region, omitting the $E_{\mathrm{T}}^{\mathrm{miss}}$ >40 GeV requirement.

Channel	Non-b-tag $\sigma_{t\bar{t}}$ (pb)	b-tag $\sigma_{t\bar{t}}$ (pb)
ee	$178 \pm 17\,^{+31\,+8}_{-34\,-7}$	$181 \pm 16\,^{+35\,+8}_{-29\,-7}$
$\mu\mu$	$159 \pm 10\,^{+20\,+7}_{-10\,-6}$	$164\,^{+11\,+18\,+7}_{-10\,-14\,-6}$
$e\mu$	$182 \pm 7\,^{+18}_{-14} \pm 8$	$193 \pm 8\,^{+20\,+8}_{-14\,-7}$
Combined	$177 \pm 6\,^{+17}_{-14} \pm 8$	$183 \pm 6\,^{+18\,+8}_{-14\,-7}$

Table 4: Measured cross-sections in each dilepton channel, and the combination of the three untagged channels and of the three tagged channels with their statistical, systematic and luminosity uncertainties.

source. The systematic variation is also modeled with Gaussian distribution, $\mathcal{G}_j$. The cross-section, $\sigma_{\rm sig}$, is left as a free parameter in the fit of the likelihood function [7]:

$$\begin{aligned}\mathcal{L}(\sigma_{\rm sig}, L, \vec{\alpha}) &= \prod_{i\in\{\rm channel\}} \mathcal{P}\left(N_i^{\rm obs} \,|\, N_{i,\rm tot}^{\rm exp}(\vec{\alpha})\right) \\ &\times \mathcal{G}(L_0|L,\sigma_L) \times \prod_{j\in\rm syst} \mathcal{G}_j(0|\alpha_j, 1)\,.\end{aligned}$$

The cross-section is extracted from the profile likelihood ratio $\lambda(\sigma_{\rm sig}) = \mathcal{L}(\sigma_{\rm sig}, \hat{\hat{L}}, \hat{\hat{\vec{\alpha}}})/\mathcal{L}(\hat{\sigma}_{\rm sig}, \hat{L}, \hat{\vec{\alpha}})$, where a single circumflex represents the maximum likelihood estimate (MLE) of the parameter and the double circumflex represents the conditional MLE for given $\sigma_{\rm sig}$. Ensembles of pseudo-data are generated for a given $N_i^{\rm obs}$ and the resulting estimate of $\hat{\sigma}_{\rm sig}$ is confirmed to be unbiased. Additionally, the variance of $\hat{\sigma}_{\rm sig}$ is found to be consistent with the curvature of the profile likelihood at its minimum and with the mean square spread observed in the ensemble tests. Table 4 summarizes the cross-sections extracted from the profile likelihood ratio for the individual channels and for the combination of all channels for the analysis with and without a b-tagging requirement, respectively.

9 Results

The top-quark pair production cross-section is measured using events selected by requiring two oppositely-charged lepton candidates, at least two additional jets and missing transverse energy. A measurement is also made requiring one of the jets to be identified as a b-quark jet.

The top-quark pair production cross-section measured without b-tagging is

$$\sigma_{t\bar{t}} = 177 \pm 6(\text{stat.})^{+17}_{-14}(\text{syst.}) \pm 8(\text{lum.})\ \text{pb}.$$

Using b-tagging, the cross-section is

$$\sigma_{t\bar{t}} = 183 \pm 6(\text{stat.})^{+18}_{-14}(\text{syst.})^{+8}_{-7}(\text{lum.})\ \text{pb}.$$

These results have been cross-checked with other techniques, confirming their robustness[2]. The cross-section results are summarized in Fig. 5.

The measured cross-sections are in good agreement with a similar measurement made with 2010 data by the CMS collaboration [38], with 2010 ATLAS measurements made in the complementary lepton+jets

[2]These two results have been updated since the EPS 2011 conference because of a correction to the W branching fraction in the signal $t\bar{t}$ MC. The old results were $\sigma_{t\bar{t}} = 171 \pm 6(\text{stat.})^{+16}_{-14}(\text{syst.}) \pm 8(\text{lum.})$ pb without b-tagging, and $\sigma_{t\bar{t}} = 177 \pm 6(\text{stat.})^{+17}_{-14}(\text{syst.}) \pm^{+8}_{-7}$ (lum.) pb with b-tagging.

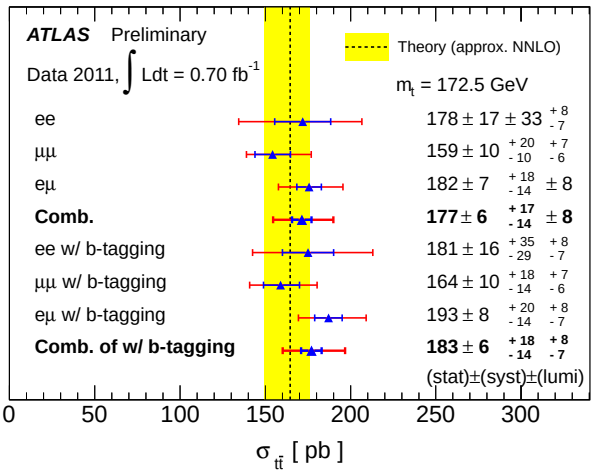

Figure 5: Cross-section summary.

channels [39, 40], with an ATLAS measurement in the dilepton channel with earlier data [7], and with the SM prediction of 165^{+11}_{-16} pb. The agreement between the measurements with and without b-tagging requirements confirms that the candidate events arise from top-quark pair production.

References

[1] S. Moch and P. Uwer, *Heavy-quark pair production at two loops in QCD*, Nucl. Phys. Proc. Suppl. **183** (2008) 75–80, arXiv:0807.2794.

[2] U. Langenfeld, S. Moch, and P. Uwer, *New Results for $t\bar{t}$ Production at Hadron Colliders*, in *XVII International Workshop on Deep-Inelastic Scattering and Related Topics, Madrid, Spain*. April, 2009. arXiv:0907.2527.

[3] CDF Collaboration, T. Aaltonen et al., *Measurement of the Top Pair Production Cross Section in the Dilepton Decay Channel in $p\bar{p}$ Collisions at $\sqrt{s}$ = 1.96 TeV*, Phys. Rev. D **82** (2010) 052002, arXiv:1002.2919.

[4] D0 Collaboration, V. M. Abazov et al., *Combination of $t\bar{t}$ Cross Section Measurements and Constraints on the Mass of the Top Quark and its Decays into Charged Higgs Bosons*, Phys. Rev. D **80** (2009) 071102, arXiv:0903.5525.

[5] CMS Collaboration, V. Khachatryan et al., *First Measurement of the Cross Section for Top-Quark Pair Production in Proton-Proton Collisions at $\sqrt{s}$ = 7 TeV*, Phys. Lett. **B695** (2011) 424, arXiv:1010.5994.

[6] ATLAS Collaboration, *Measurement of the top quark-pair production cross-section with ATLAS in pp collisions at $\sqrt{s}$ = 7 TeV*, Eur. Phys. Journal C **71** (2011) 1, arXiv:1012.1792.

[7] ATLAS Collaboration, *Measurement of the top quark pair production cross section with ATLAS in pp collisions at $\sqrt{s}$ = 7 TeV in dilepton final states*, ATLAS-CONF-2011-034 (2011) .

[8] ATLAS Collaboration, *ATLAS Experiment at the CERN Large Hadron Collider*, JINST **3** (2008) S08003.

[9] ATLAS Collaboration, *Updated Luminosity Determination in pp Collisions at $\sqrt{s}$ = 7 TeV using the ATLAS Detector*, ATLAS-CONF-2011-011 (2011) .

[10] GEANT4 Collaboration, S. Agostinelli et al., *GEANT4: A simulation toolkit*, Nucl. Instrum. Meth. **A506** (2003) 250.

[11] ATLAS Collaboration, *ATLAS Simulation Infrastructure*, Eur. Phys. J. **C70** (2010) 823, arXiv:1005.4568.

[12] S. Frixione and B. R. Webber, *Matching NLO QCD computations and parton shower simulations*, JHEP **06** (2002) 029, arXiv:hep-ph/0204244. We use Version 3.41.

[13] S. Frixione, P. Nason, and B. R. Webber, *Matching NLO QCD and parton showers in heavy flavour production*, JHEP **08** (2003) 007, arXiv:hep-ph/0305252.

[14] S. Frixione, E. Laenen, P. Motylinski, and B. R. Webber, *Single-top production in MC@NLO*, JHEP **03** (2006) 092, arXiv:hep-ph/0512250.

[15] P. M. Nadolsky et al., *Implications of CTEQ global analysis for collider observables*, Phys. Rev. D **78** (2008) 013004, arXiv:0802.0007.

[16] M. Aliev et al., – *HATHOR – HAdronic Top and Heavy quarks crOss section calculatoR*, Comput. Phys. Commun. **182** (2011) 1034, arXiv:1007.1327.

[17] S. Frixione, E. Laenen, P. Motylinski, B. R. Webber, and C. D. White, *Single-top hadroproduction in association with a W boson*, JHEP **07** (2008) 029, arXiv:0805.3067.

[18] M. L. Mangano, M. Moretti, F. Piccinini, R. Pittau, and A. D. Polosa, *ALPGEN, a generator for hard multiparton processes in hadronic collisions*, JHEP **07** (2003) 001, arXiv:hep-ph/0206293. We use version 2.13.

[19] J. Pumplin, D. Stump, J. Huston, H. Lai, P. Nadolsky, and W. Tung, *New generation of parton distributions with uncertainties from global QCD analysis*, JHEP **07** (2002) 012, arXiv:hep-ph/0201195.

[20] ATLAS Collaboration, *Expected Performance of the ATLAS Experiment - Detector, Trigger and Physics*, arXiv:0901.0512.

[21] G. Corcella et al., *HERWIG 6.5: an event generator for Hadron Emission Reactions With Interfering Gluons (including supersymmetric processes)*, JHEP **01** (2001) 010, arXiv:hep-ph/0011363. We use version 6.510.

[22] G. Corcella et al., *HERWIG 6.5 release note*, arXiv:hep-ph/0210213.

[23] J. M. Butterworth, J. R. Forshaw, and M. H. Seymour, *Multiparton interactions in photoproduction at HERA*, Z. Phys. **C72** (1996) 637, arXiv:hep-ph/9601371. We use version 4.31.

[24] ATLAS Collaboration, *First tuning of HERWIG/JIMMY to ATLAS data*, ATL-PHYS-PUB-2010-014 (2010) .

[25] J. M. Campbell and R. K. Ellis, *An update on vector boson pair production at hadron colliders*, Phys. Rev. D **60** (1999) 113006, arXiv:hep-ph/9905386.

[26] ATLAS Collaboration, *Measurement of the $W \to l\nu$ and $Z/\gamma^* \to ll$ production cross sections in pp collisions at $\sqrt{s}$ = 7 TeV with the ATLAS detector*, JHEP **12** (2010) 060, arXiv:1010.2130.

[27] M. Cacciari, G. P. Salam, and G. Soyez, *The Anti-K_T Jet Clustering Algorithm*, JHEP **0804** (2008) 063, arXiv:0802.1189.

[28] ATLAS Collaboration, *Measurement of inclusive jet and dijet cross sections in proton-proton collisions at 7 TeV centre-of-mass energy with the ATLAS detector*, Eur. Phys. J. **C71** (2011) 1512, arXiv:1009.5908.

[29] ATLAS Collaboration, *Data-Quality Requirements and Event Cleaning for Jets and Missing Transverse Energy Reconstruction with the ATLAS Detector in Proton-Proton Collisions at a Center-of-Mass Energy of $\sqrt{s}$ = 7 TeV*, ATLAS-CONF-2010-038 (2010) .

[30] ATLAS Collaboration, *Jet energy scale and its systematic uncertainty in proton-proton collisions at $\sqrt{s}$ = 7 TeV in ATLAS 2010 data*, ATLAS-CONF-2011-032 (2011) .

[31] P. Nason, *A new method for combining NLO QCD with shower Monte Carlo algorithms*, JHEP **11** (2004) 040, arXiv:hep-ph/0409146.

[32] S. Frixione, P. Nason, and C. Oleari, *Matching NLO QCD computations with Parton Shower simulations: the POWHEG method*, JHEP **11** (2007) 070, arXiv:0709.2092.

[33] S. Alioli, P. Nason, C. Oleari, and E. Re, *A general framework for implementing NLO calculations in shower Monte Carlo programs: the POWHEG BOX*, JHEP **06** (2010) 043, arXiv:1002.2581.

[34] B. P. Kersevan and E. Richter-Was, *The Monte Carlo event generator AcerMC version 2.0 with interfaces to PYTHIA 6.2 and HERWIG 6.5*, arXiv:hep-ph/0405247.

[35] J. M. Campbell, R. K. Ellis, and F. Tramontano, *Single top production and decay at next-to-leading order*, Phys. Rev. D **70** (2004) 094012, arXiv:hep-ph/0408158.

[36] N. Kidonakis, *Single top quark production cross section at hadron colliders*, PoS DIS2010 (2010) 196, arXiv:1005.3330.

[37] J. M. Campbell and R. K. Ellis, *MCFM for the Tevatron and the LHC*, Nucl. Phys. Proc. Suppl. **205** (2010) 10, arXiv:1007.3492.

[38] CMS Collaboration, S. Chatrchyan et al., *Measurement of the $t\bar{t}$ production cross section and the top quark mass in the dilepton channel in pp collisions at $\sqrt{s}$ = 7 TeV*, arXiv:1105.5661.

[39] ATLAS Collaboration, *Top Quark Pair Production Cross-section Measurements in ATLAS in the Single Lepton+Jets Channel without b-tagging*, ATLAS-CONF-2011-023 (2011) .

[40] ATLAS Collaboration, *Measurement of the top quark-pair cross-section with ATLAS in pp collisions at $\sqrt{s}$ = 7 TeV in the single-lepton channel using b-tagging*, ATLAS-CONF-2011-035 (2011) .

10 Appendix

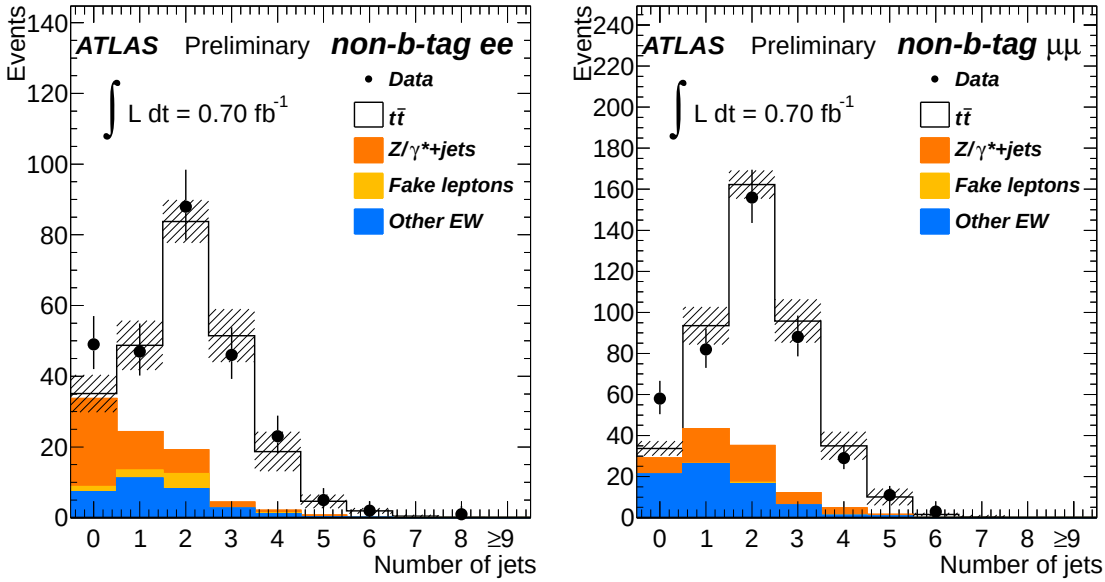

(a) (b)

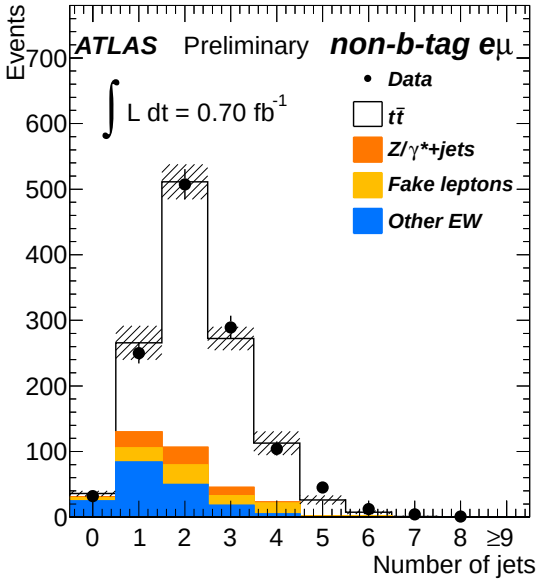

(c)

Figure 6: Jet multiplicity distribution for the non-b-tag signal region, omitting the $N_{jets} > 2$ requirement.

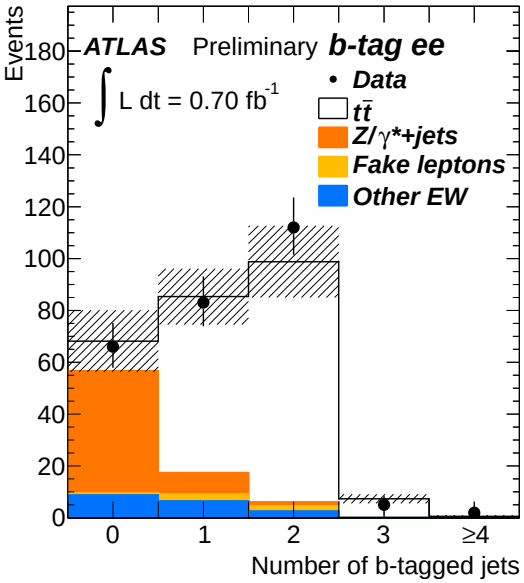

(a)

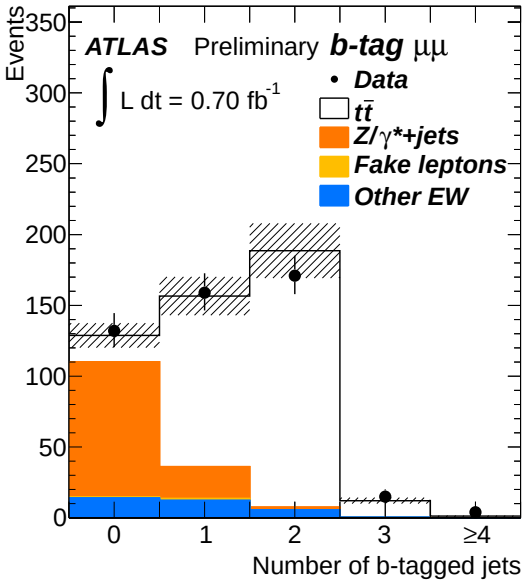

(b)

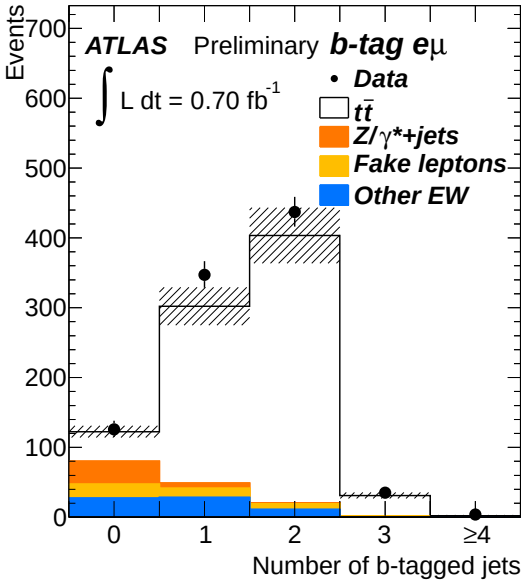

(c)

Figure 7: Number of *b*-tagged jets in the *b*-tag analysis signal region, omitting the requirement of at least one *b*-tagged jet.